Brazilian Journal
of Chemical
Engineering

ISSN 0104-6632
Printed in Brazil
www.abeq.org.br/bjche

Vol. 31, No. 04, pp. 829 - 838, October - December, 2014
dx.doi.org/10.1590/0104-6632.20140314s00002871

THE EFFECT OF THE INNER CYLINDER ROTATION ON THE FLUID DYNAMICS OF NON-NEWTONIAN FLUIDS IN CONCENTRIC AND ECCENTRIC ANNULI

J. L. Vieira Neto[1], A. L. Martins[2], C. H. Ataíde[1] and M. A. S. Barrozo[1*]

[1]Department of Chemical Engineering, Federal University of Uberlandia, Building 1K,
Campus Santa Monica, POB 593, 38400-902, Uberlandia - MG, Brazil.
E-mail: masbarrozo@ufu.br
[2] PETROBRAS R&D Center, Well Technology Sector, 21949-900, Rio de Janeiro - RJ, Brazil.

(Submitted: July 24, 2013 ; Revised: October 25, 2013 ; Accepted: December 8, 2013)

Abstract - Helical flow in an annular space occurs during oil drilling operations. The correct prediction of flow of drilling fluid in an annular space between the wellbore wall and the drill pipe is essential to determine the variation in fluid pressure within the wellbore. This paper presents experimental and CFD simulation results of the pressure drop in the flow of non-Newtonian fluids through a concentric annular section and another section with fixed eccentricity (E = 0.75), using aqueous solutions of two distinct polymers (Xanthan Gum and Carboxymethylcellulose). The hydrodynamic behavior in this annular system was analyzed based on the experimental and CFD results, providing important information such as the formation of zones with preferential flows and stagnation regions.
Keywords: Annular spaces; Fluid-dynamics; Velocity profiles.

INTRODUCTION

The petroleum industry has shown increasing interest in studies of fluid dynamics in annular spaces, involving oil well drilling operations with cuttings removal using drilling fluids. Constant concerns regarding operational costs and the need to increase production capacity have often led to the use of high flow rates, with the resulting hydrodynamic losses in the annular space between the wellbore and drill pipe requiring significant amounts of energy (Vieira Neto *et al*., 2011). The quantification of this energy therefore plays a relevant role in the dimensioning of these units.

Cuttings are removed by pumping drilling fluids from the surface into the wellbore through the inside of drill pipe to lubricate and cool the drill bit and clean the cut region, thus avoiding unnecessary increases in the required torque due to the accumulation of particles (Nouri and Whitelaw, 1997). The drag of these particles is strongly related to the flow of drilling fluid, which is determined by the velocity profiles in the annular space (Escudier *et al*., 2000). Therefore, efficient drilling operations are directly dependent on knowledge about *drilling fluid hydraulics*.

The work of Nouri *et al*. (1993) stands out among experimental studies on turbulent flow in annular sections. These authors analyzed turbulent flow in vertical annular sections (concentric and eccentric) without the effect of rotation of the inner cylinder. They used Newtonian fluids and non-Newtonian solutions (0.2% CMC), determining the mean velocity profiles (axial, radial and tangential) and their fluctuations and cross-correlations by means of the

*To whom correspondence should be addressed

LDV technique (Laser Doppler Velocimetry). They also calculated the skin friction coefficients for both fluids, and highlighted the reduction of about 7% in pressure drop due to increased eccentricity.

Nouri and Whitelaw (1994) continued their earlier experimental studies (Nouri *et al*., 1993) on vertical turbulent flows in a concentric annulus, this time including rotation of the inner tube (300 rpm). Newtonian and non-Newtonian fluids were also used in that study, and the mean velocity profiles (axial, radial and tangential) and their fluctuations were determined by the LDV technique. Later, Nouri and Whitelaw (1997) extended their studies to an eccentric annular section with inner cylinder rotation (300 rpm), and found that the influence of rotation of the inner cylinder is more significant in the range of $Re_G < 3000$, and this influence is lower on turbulent flows.

Escudier and Gouldson (1995) also engaged in experimental studies of the flow of Newtonian and pseudoplastic fluids under the influence of rotation of the central body, using LDA (Laser Doppler Anemometry) as the measuring technique. They plotted velocity profiles for different flow situations (fluid flow rate and inner cylinder rotation), and also highlighted the behavior of the friction factor as a function of fluid flow rate. Glucose syrup solutions were used as the Newtonian fluid and carboxymethylcellulose (CMC) solutions as the non-Newtonian fluid.

Escudier *et al*. (2000) evaluated the effect of inner cylinder rotation on the laminar flow of Newtonian fluids in an eccentric annular region and described the effect of the friction factor under the influence of flow conditions and eccentricity. Escudier *et al*. (2002) extended the study to non-Newtonian fluids, comparing experimental and numerical simulation results and highlighting the velocity profiles, which they compared with those obtained in other studies reported in the literature (Nouar *et al*., 1987; Nouri and Whitelaw, 1997).

Fang *et al*. (1999) proposed numerical simulations using the finite difference technique to study the flow of pseudoplastic fluids in an eccentric annulus. They discussed the effects of eccentricity and viscosity on the friction factor associated with flow, and compared their results with those reported by other authors (Nouri *et al*., 1993; Nouri and Whitelaw, 1997).

Today, with the rapid improvement of computational resources, numerical simulation studies using the Computational Fluid Dynamics (CFD) technique have become popular in several fields of engineering (Vieira *et al*., 2005; Vieira Neto *et al*., 2008; Cunha *et al*., 2009; Barrozo *et al*., 2010, Santos *et al*., 2009, Oliveira *et al*., 2009, Pereira *et al*., 2007), helping to shed light on the fluid dynamic behavior of annular flows.

Fisher *et al*. (2000) incorporated the effect of porosity at the system's boundary into their simulations. Their aim was to determine the fluid dynamics of the flow to predict the loss behavior of drilling fluids and the thickness of the cake formed on the wellbore wall, considering the influence of eccentricity and internal shaft rotation. They reported results consistent with information available in the literature, but did not compare their numerical results with experimental data.

Ali (2002) estimated concentric annular flows of Newtonian fluids in vertical and horizontal arrangements based on CFD simulations, but did not quantify the effects of internal shaft rotation.

The above-mentioned studies indicate that there is a need for studies that combine experimental work and CFD simulations to investigate pressure gradients, in concentric and eccentric annuli, of flows of different non-Newtonian fluids, evaluating their effects on the hydrodynamics of these systems. Furthermore, it is also important to evaluate velocity fields in order to identify areas of preferential flows and stagnation zones, because they directly affect the flow of drilling fluid in real well drilling situations.

In the present work, CFD simulations and experimental studies were performed to analyze the pressure drop in concentric and eccentric annuli, with and without inner tube rotation, using aqueous solutions of two polymers (0.2% Xanthan gum and 0.2% carboxymethylcellulose) to assess the differences in non-Newtonian behavior of these fluids and their effect on the hydrodynamics of these annular systems. This work also involved CFD simulations to determine velocity profiles and identify the presence of preferential flows and stagnation zones, particularly in the eccentric annulus.

MATERIALS AND METHODS

Experimental Methodology

The rheological data of non-Newtonian fluids were best fitted by the power law model. The rheological data of aqueous suspensions of 0.2% Xanthan Gum (XG) and of 0.2% carboxymethylcellulose (CMC) were measured using a Brookfield rheometer at a temperature of 25 °C (Ataíde *et al*., 1999). The *power law* model can be expressed by Eq. (1):

$$\tau = \mathrm{K}\left(\dot{\gamma}\right)^{\mathrm{n}} \tag{1}$$

Table 1 shows the *power-law* parameters obtained by regression for both fluids, using a range of shear rate $(\dot{\gamma})$ from 0 to 80 s^{-1} to determine the parameters.

Figure 1 illustrates the experimental apparatus used in this study. The annular region is composed of two cylindrical bodies: an external acrylic tube (67 mm in diameter) and an internal stainless steel tube (32 mm in diameter), both 1.5 m long. The ratio of the diameters is 0.48.

The fluids were moved using a helical pump (7.5 hp), while the flow rate was quantified using a magnetic flow meter. The rotation of the inner tube was adjusted by a frequency inverter. The working fluids were fed into the annular region using a flange to support the arrangement between the inner and outer tubes. This device allowed the main flow to be diverted to different positions around the annular section through a flow distributor. The fluid discharge system followed the same principle as the feeding device. Each pair of flanges, when attached to the acrylic tube, allowed the inner shaft to be positioned to provide concentric and eccentric arrangements (with fixed eccentricity, E = 0.75).

The pressure measuring points were distributed along the length of the outer tube. In the eccentric arrangement, the pressure drops were measured in the section with the largest annular space. To evaluate the effect of the inner shaft rotation on the pressure drop, several experiments were performed at a fluid flow rate of 6.8 m^3/h in the following arrangements: concentric without rotation and with inner shaft rotation (300 rpm), and eccentric (E = 0.75) without rotation and with inner shaft rotations (150 and 200 rpm).

Simulation Methodology

The procedure for the numerical simulation was implemented using the ANSYS FLUENT© 12.1 CFD package, while the grid was constructed using GAMBIT© 2.3.16 software.

Table 1: Parameters of the power law model for the two fluids.

non-Newtonian fluids	Parameters of the power law model		
	K [Pa.s^n]	n [–]	R^2
0.2% XG solution	0.678	0.27	0.95
0.2% CMC solution	0.096	0.75	0.94

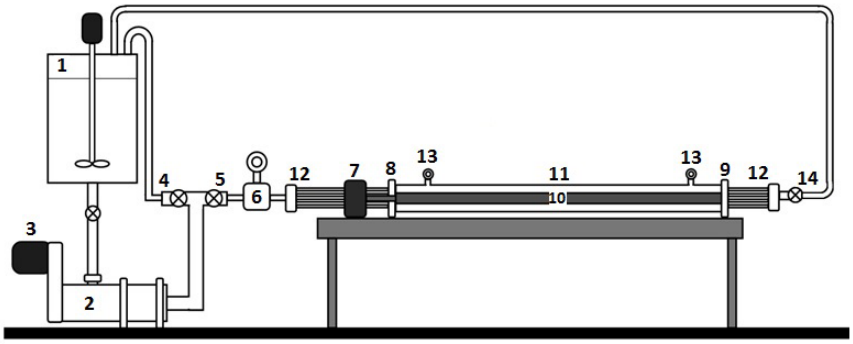

Figure 1: Experimental apparatus: (1) Fluid tank; (2) Helical pump of positive displacement; (3) Motor of 7.5 hp for the helical pump; (4) and (5) Valve of bypass and hose; (6) Magnetic flowmeter; (7) Motor of 1.0 hp to rotate the inner tube; (8) Input flange; (9) Output flange; (10) Inner tube of stainless steel; (11) External tube of acrylic; (12) Flow distributors with silicone hoses; (13) Points for pressure measurement; (14) Valve of recycling and hose.

Governing Equations

For an incompressible isothermal laminar flow of a fluid whose effective viscosity depends solely on the strain rate tensor, the modeling of the flow can be described through the continuity equation (Equation (2)), using axial, radial and tangential components of the momentum equation (Equations (3), (4) and (5)) in cylindrical coordinates (Bird *et al*., 2002).

$$\frac{\partial \rho}{\partial t}+\frac{1}{r}\frac{\partial}{\partial r}(\rho r v_r)+\frac{1}{r}\frac{\partial}{\partial \theta}(\rho v_\theta)+\frac{\partial}{\partial z}(\rho v_z)=0 \tag{2}$$

$$\rho\left(\frac{\partial v_z}{\partial t}+v_r\frac{\partial v_z}{\partial r}+\frac{v_\theta}{r}\frac{\partial v_z}{\partial \theta}+v_z\frac{\partial v_z}{\partial z}\right)= -\frac{\partial P}{\partial z}+\mu\left[\frac{1}{r}\frac{\partial}{\partial r}\left(r\frac{\partial v_z}{\partial r}\right)+\frac{1}{r^2}\frac{\partial^2 v_z}{\partial \theta^2}+\frac{\partial^2 v_z}{\partial z^2}\right]+\rho g_z \tag{3}$$

$$\rho\left(\frac{\partial v_r}{\partial t}+v_r\frac{\partial v_r}{\partial r}+\frac{v_\theta}{r}\frac{\partial v_r}{\partial \theta}+v_z\frac{\partial v_r}{\partial z}-\frac{v_\theta^2}{r}\right)=-\frac{\partial P}{\partial r} +\mu\left[\frac{\partial}{\partial r}\left(\frac{1}{r}\frac{\partial}{\partial r}(r v_r)\right)+\frac{1}{r^2}\frac{\partial^2 v_r}{\partial \theta^2}+\frac{\partial^2 v_r}{\partial z^2}-\frac{2}{r^2}\frac{\partial v_\theta}{\partial \theta}\right]+\rho g_r \tag{4}$$

$$\rho\left(\frac{\partial v_\theta}{\partial t}+v_r\frac{\partial v_\theta}{\partial r}+\frac{v_\theta}{r}\frac{\partial v_\theta}{\partial \theta}+v_z\frac{\partial v_\theta}{\partial z}+\frac{v_r v_\theta}{r}\right)=-\frac{1}{r}\frac{\partial P}{\partial \theta} +\mu\left[\frac{\partial}{\partial r}\left(\frac{1}{r}\frac{\partial}{\partial r}(r v_\theta)\right)+\frac{1}{r^2}\frac{\partial^2 v_\theta}{\partial \theta^2}+\frac{\partial^2 v_\theta}{\partial z^2}+\frac{2}{r^2}\frac{\partial v_r}{\partial \theta}\right]+\rho g_\theta \tag{5}$$

Considering the *power law* rheological model (Eq. (1)), the effective viscosity (μ_E) concept has been used in the present work. Thus, we use the effective viscosity to replace the dynamic viscosity (μ) in these equations. The parameters of this model (Table 1) were implemented in FLUENT© 12.1 software.

Grid and Simulation Parameters

In the construction of the grid, the cells adjacent to the walls of the inner and outer tubes, as well as those in the regions of entry and exit of fluid, were refined through a double-side scheme with a cells growth factor of 1.1. A grid independence test was carried out with three different grid sizes. A grid with 192,000 cells and 20x80x120 subdivisions (radial, circumferential and axial) was chosen because this grid gave a grid-independent solution.

Figures 2 and 3 show the refinement of the grid along the annular section and in the region of entry of the concentric and eccentric annuli (E = 0.75).

The simulations were performed in the steady-state regime, with convergence criteria of $1e^{-4}$. The algorithm SIMPLE was used for coupling pressure-velocity, the scheme PRESTO for the pressure discretization, and the scheme QUICK for the discretization of the equations of motion. The boundary conditions adopted were an axial velocity of 0.69 m/s at the entrance of the section (corresponding to a volumetric flow rate of 6.8 m^3/h in the experimental tests) and rotation speeds of 300 rpm in the concentric channel of the inner tube, and of 150 and 200 rpm in the eccentric annulus.

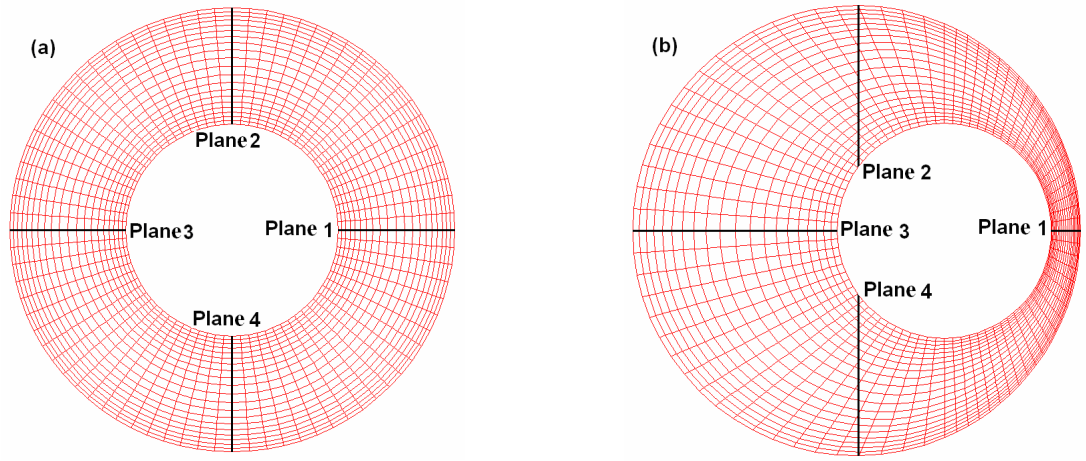

Figure 2: Grid refinement along the annular section: (a) concentric; (b) eccentric (E = 0.75).

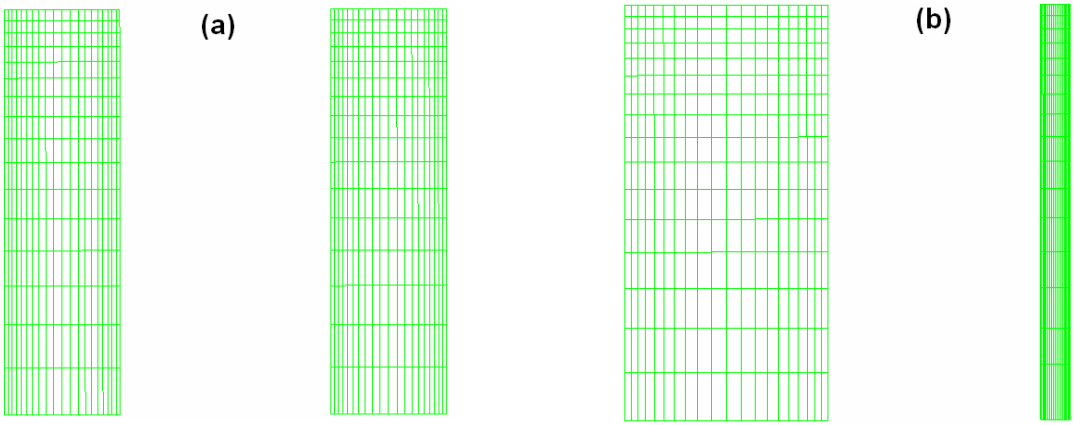

Figure 3: Grid refinement in the intake region: (a) concentric; (b) eccentric (E = 0.75).

RESULTS AND DISCUSSION

Results for the Experimental and Simulated Pressure Drop

Figure 4 indicates that the introduction of the inner cylinder rotation (300 rpm) in the concentric annulus reduces the pressure drop slightly: XG (reduction of 4.1%) and CMC (reduction of 1.2%). It also can be seen that the fluctuation of the experimental measurements for CMC is higher than that for XG. The simulated values over-predict the mean values of the experimental data, but are within the error bar.

Figure 5 shows that, in the eccentric annulus, the introduction of the inner cylinder rotation (up to 200 rpm) increases the pressure drop: XG (increase of 10.2%) and CMC (increase of 5.9%), indicating an opposite effect to that found in the concentric channel. Likewise, the simulated values over-predict the mean values of the experimental data, although they are within the experimental error bar.

Simulated Profiles of Normalized Axial and Tangential Velocities

Figure 6 depicts the simulated profiles of the radial distribution of the axial (Figure 6-a) and tangential (Figure 6-b) velocity normalized by the bulk velocity (U_b = 0.69 m/s), of the two polymer solutions (0.2% XG and 0.2% CMC) in the concentric annulus at a flow rate of 6.8 m^3/h. In these figures, r1 is the radial distance from the outer cylinder, while S is the annular space between the inner and outer tubes.

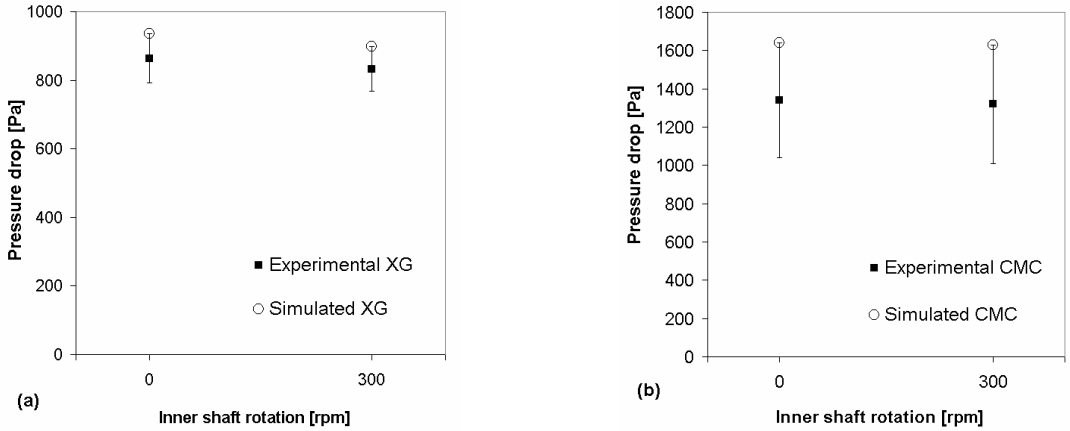

Figure 4: Experimental pressure drop (mean and standard deviation) and mean simulated values in the concentric annulus: (a) 0.2% XG, (b) 0.2% CMC.

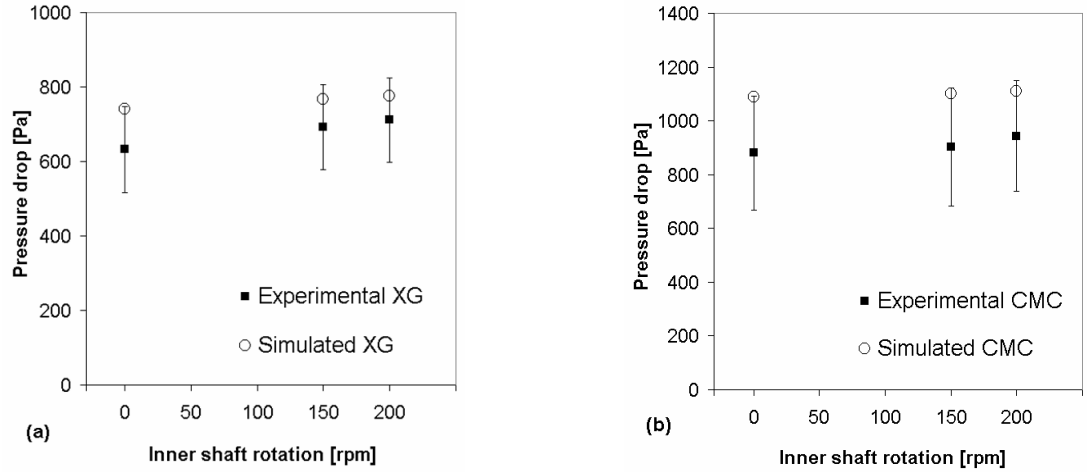

Figure 5: Experimental pressure drop (mean and deviation) and mean simulated values in the eccentric annulus: (a) 0.2% XG, (b) 0.2% CMC.

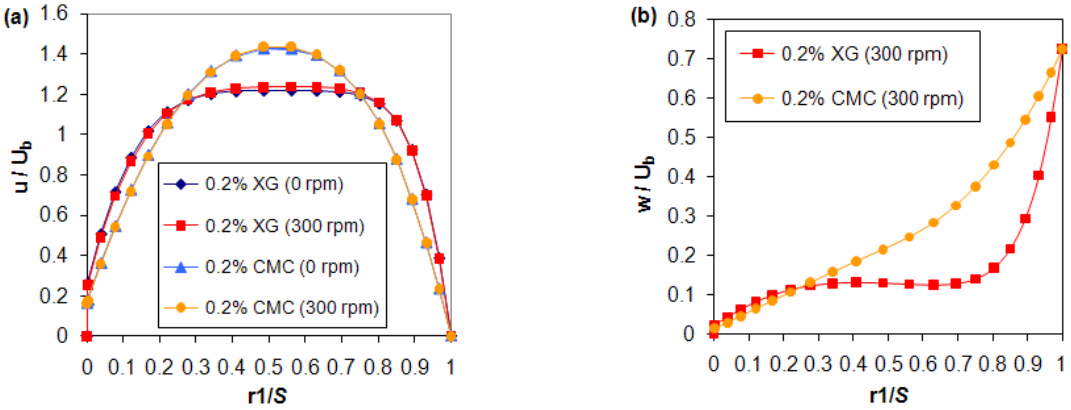

Figure 6: Simulated profiles of velocities normalized by bulk velocity (U_b) for both fluids (0.2% XG and 0.2% CMC) in the concentric annulus: (a) axial velocity; (b) tangential velocity.

In Figure 6(a), note that there are significant differences in the profiles of normalized axial velocities due to the rheological characteristics of the fluids. The 0.2% CMC solution, whose behavior index (n = 0.749) is closer to a Newtonian fluid (n = 1), presents a parabolic velocity profile, while the 0.2% XG solution with the lower behavior index (n = 0.27), i.e., with more evident characteristics of a pseudoplastic fluid, displays a flattened profile. Note also that the increment in rotation of the inner tube (300 rpm) practically did not interfere in the axial velocity profiles.

As can be seen in Figure 6(b), tangential velocity decreased sharply as the fluid moved away from the inner cylinder (normalized radial position equal to 1), in the case of the 0.2% XG solution, whose non-Newtonian behavior is more evident. In contrast, the tangential velocity of the 0.2% CMC solution decreased more gradually.

Figures 7 to 10 illustrate the simulated radial distribution profiles of axial and tangential velocities normalized by the bulk velocity (U_b) of the two solutions (0.2% XG and 0.2% CMC) in the eccentric arrangement (E = 0.75).

In the case of the larger annular space (plane 3) of the eccentric arrangement, Figure 7(b) shows that the simulated axial velocity profiles of the XG solution were flat while those of the CMC solution were parabolic. This behavior was similar to that of the concentric annulus (Figure 6-a). Figure 7(a), which depicts the narrowest region (plane 1), shows that the introduction of the inner tube rotation (up to 200 rpm) increased significantly the axial flow in this region. This increment in axial flow in plane 1 decreased the stagnation of the flow due to the high eccentricity of the annulus. This effect is relevant in cleaning operations and the transportation of cuttings in horizontal drilling systems.

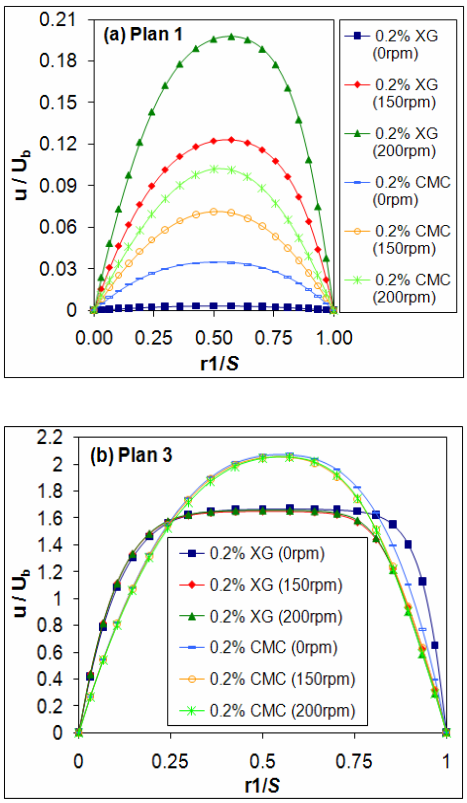

Figure 7: Radial distribution of simulated profiles of axial velocities, for both fluids, in the eccentric annulus (E = 0.75): (a) plane 1, (b) plane 3.

Figure 8(a) shows the simulated profiles of axial velocities in the region of plane 2 of the eccentric annulus for both fluids. The simulated results without the inner tube rotation presented higher values close to the inner cylinder (normalized radial position equal to 1). Note also that the insertion of inner cylinder rotation (150 and 200 rpm) reversed the trend of the velocity profiles, which became elevated close to the wall of the outer cylinder, but with lower values than those obtained without inner tube rotation.

Figure 8(b) shows that the two fluids behaved differently in the simulated axial velocity profiles of plane 4. The XG solution showed a behavior similar to plane 2, but increasing the inner tube rotation (up to 200 rpm) caused an increase in the axial velocity values adjacent to the wall of the outer cylinder. In the case of the CMC solution, also note that the insertion of inner tube rotation increased the axial velocities, but these higher values are located in the central region of the annulus. This increase in axial flow in plane 4 (bottom region of the annulus) due to inner tube rotation also facilitates the cleaning operations and transportation of cuttings, since it prevents the deposition of solids at the bottom of the annulus.

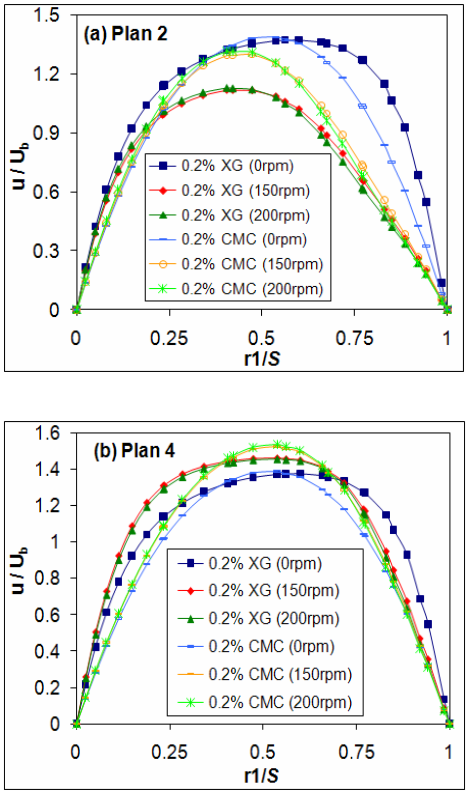

Figure 8: Radial distribution of simulated profiles of axial velocities of the two fluids in the eccentric annulus (E = 0.75): (a) plane 2, (b) plane 4.

Figure 9(a) exhibits the simulated tangential velocity profiles in the narrowest region of the annulus (plane 1). A gradual decrease in tangential velocity was observed when the fluid deviated from the inner cylinder (normalized radial position equal to 1), although this decrease was more gradual with the CMC solution than with the XG solution. In Figure 9(b), note that the tangential velocity of both solutions declined sharply in the region of larger annular space (plane 3) as the fluid moved away from the inner cylinder (normalized radial position equal to 1). An inflection point was also observed in the center of the annular section, where the tangential velocities became negative. These negative values may indicate a minor secondary flow in the direction opposite to that of the inner tube rotation, particularly in the case of the CMC solution. A possible physical explanation for this secondary flow could be the high eccentricity (E = 0.75) associated with the rheological characteristics of non-Newtonian fluids.

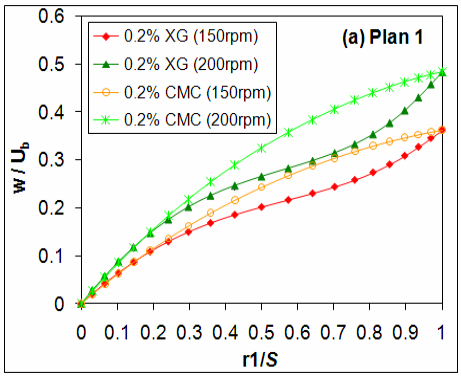

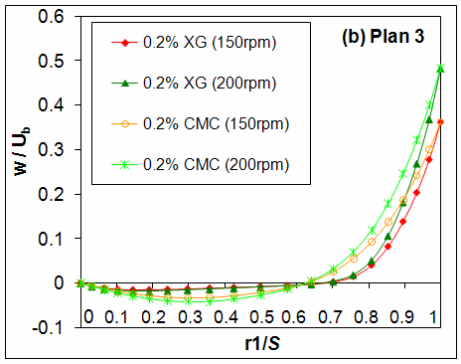

Figure 9: Simulated profiles of tangential velocities of the two fluids in the eccentric annulus (E = 0.75): (a) plane 1, (b) plane 3.

In Figure 10, note that the behavior of the tangential velocity profiles in planes 2 and 4 was similar to that in plane 3 (higher annular space). The two fluids showed an abrupt decrease in tangential velocity as they approached the center of the annulus, and an inversion in velocity values. These negative values may also indicate a small secondary flow in the direction opposite to that of the inner tube rotation, which is especially evident in Figure 10(b) (plane 4).

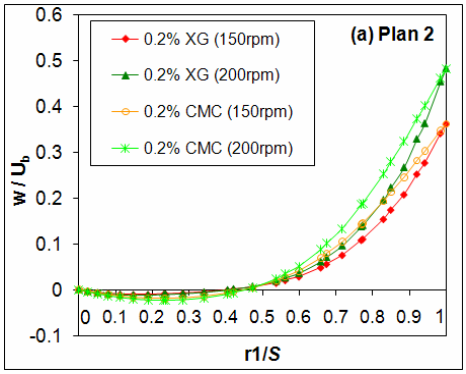

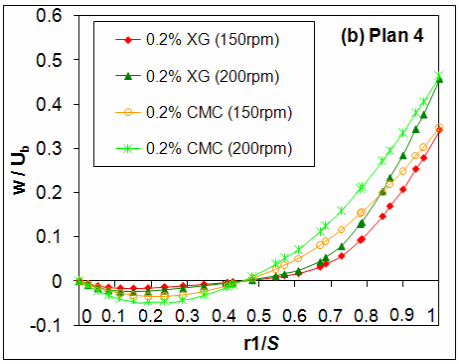

Figure 10: Simulated profiles of tangential velocities of the two fluids in the eccentric annulus (E = 0.75): (a) plane 2, (b) plane 4.

CONCLUSIONS

In this work, CFD and experimental studies were conducted to analyze the pressure drop in concentric and eccentric annuli, with and without inner tube rotation, using aqueous solutions of two polymers (0.2% Xanthan gum and 0.2% carboxymethylcellulose)

The experimental and simulated results of the two fluids showed a decrease in pressure drop with inner cylinder rotation in the concentric annulus. The opposite effect was found to occur in the eccentric arrangement, i.e., the introduction of the inner tube rotation increased the pressure drop of both fluids.

The simulated axial velocity profiles in the concentric annulus were flat for the XG solution and parabolic for the CMC solution. The simulated tangential velocity profiles showed a sudden decrease in tangential velocity of the XG solution as it moved away from the inner cylinder, while this decrease was more gradual with the CMC solution.

The simulated axial velocities in the larger annular space (plane 3) of the eccentric arrangement showed a behavior similar to that observed in the concentric annulus, i.e., the profiles of the XG solution were flat while those of the CMC solution were parabolic, due to the rheological characteristics of these fluids. In the narrowest region of the eccentric annulus (plane 1), it was found that the introduction of inner cylinder rotation increased the axial flow in this region, where previously there was no axial flow. In the other planes of the eccentric arrangement, the introduction of inner tube rotation reduced the axial velocity in plane 2, and increased the axial velocity in plane 4.

The narrowest region of the annulus (plane 1) showed a gradual decrease in tangential velocity as

the fluid moved away from the inner tube, although this decrease was more gradual with the CMC solution. The other regions of the annulus (planes 2, 3 and 4) showed a sudden decrease in tangential velocity as the fluid approached the center of the annulus, after which the values became negative. Negative values of tangential velocity may indicate a minor secondary flow in the direction opposite to that of the inner tube rotation.

ACKNOWLEDGEMENTS

The authors acknowledge the financial support provided through an agreement between CENPES/ PETROBRAS and FAU/UFU.

NOMENCLATURE

E	eccentricity	(-)
g_z, g_r, g_θ	gravity in cylindrical coordinates	m/s^2
K	consistency index of the "power-law" model	$Pa.s^n$
n	behavior index of the "power-law" model	(-)
P	pressure	Pa
r1	radial distance from the outer cylinder	m
S	annular space between the inner and outer tubes	m
t	time	s
u	simulated axial velocity	m/s
U_b	*bulk* velocity of the fluid flow	m/s
v_z, v_r, v_θ	velocity in cylindrical coordinates	m/s^2
w	simulated tangential velocity	m/s
z, r, θ	cylindrical coordinates (axial, radial and angular) of the momentum equations	

Greek Symbols

$\dot{\gamma}$	characteristic strain rate	s^{-1}
μ	dynamic viscosity of the Newtonian fluids	Pa.s
ρ	fluid density	kg/m^3
τ	shear stress	Pa

REFERENCES

Ali, W. A., Parametric study of cutting transport in vertical and horizontal well using computational fluid dynamics (CFD). M. Sc. Thesis, Department of Petroleum and Natural Gas Engineering, West Virginia University, United States (2002).

Ataíde, C. H., Pereira, F. A. R., Barrozo, M. A. S., Wall effects on the terminal velocity of spherical particles in Newtonian and non-Newtonian fluids. Braz. J. Chem. Eng., 16, 387-394 (1999).

Barrozo, M. A. S., Duarte, C. R., Epstein, N., Grace, J. R., Lim, C. J., Experimental and computational fluid dynamics study of dense-phase, transition region and dilute-phase spouting. Ind. Eng. Chem., 49, 5102-5109 (2010).

Bird, R. B., Stewart, W. E., Lightfoot, E. N., Transport Phenomena. Second Edition, John Wiley & Sons Inc., New York (2002).

Cunha, F. G., Santos, K. G., Ataíde, C. H., Epstein, N., Barrozo, M. A. S., Annatto powder production in a spouted bed: An experimental and CFD study. Ind. Eng. Chem. Res., 48, 976-982 (2009).

Escudier, M. P., Gouldson, I. W., Concentric annular flow with center body rotation of a Newtonian and a shear-thinning liquid. Int. J. Heat Fluid Flow, 16, 156-162 (1995).

Escudier, M. P., Gouldson, I. W., Oliveira, P. J., Pinho, F. T., Effects of inner cylinder rotation on laminar flow of a Newtonian fluid through an eccentric annulus. Int. J. Heat Fluid Flow, 21, 92-103 (2000).

Escudier, M. P., Oliveira, P. J., Pinho, F. T., Fully developed laminar flow of purely viscous non-Newtonian liquids through annuli, including effects of eccentricity and inner-cylinder rotation. Int. J. Heat Fluid Flow, 23, 52-73 (2002).

Fang, P., Manglik, R. M., Jog, M. A., Characteristics of laminar viscous shear-thinning fluid flows in eccentric annular channels. J. Non-Newtonian Fluid Mech., 84, 1-17 (1999).

Fisher, K. A., Wakeman, R. J., Chiu, T. W., Meuric, O. F. J., Numerical modeling of cake formation and fluid loss from non-Newtonian muds during drilling using eccentric/concentric drill strings with/ without rotation. Chem. Eng. Res. Des., 78, 707-714 (2000).

Nouar, C., Devienne, R., Lebouché, M., Thermal convection for Couette flow with axial flow rate. Case of a pseudo-plastic fluid. Int. J. Heat Mass Transfer, 30, 639-647 (1987).

Nouri, J. M., Umur, H., Whitelaw, J. H., Flow of Newtonian and non-Newtonian fluids in concentric and eccentric annuli. J. Fluid. Mech., 253, 617-641 (1993).

Nouri, J. M., Whitelaw, J. H., Flow of Newtonian and non-Newtonian fluids in a concentric annulus with rotation of the inner cylinder, J. Fluid. Eng., 116, 821-827 (1994).

Nouri, J. M., Whitelaw, J. H., Flow of Newtonian and non-Newtonian fluids in an eccentric annulus with the rotation of the inner cylinder. Int. J. Heat and Fluid Flow, 18, 236-246 (1997).

Oliveira, D. C., Almeida, C. A. K., Vieira, L. G. M., Damasceno, J. J. R., Barrozo, M. A. S., Influence of geometric dimensions on the performance of a filtering hydrocyclone: An experimental and CFD study. Braz. J. Chem. Eng., 26(3), 575-582 (2009).

Pereira, F. A. R., Barrozo, M. A. S., Ataíde, C. H., CFD predictions of drilling fluid velocity and pressure profiles in laminar helical flow. Braz. J. Chem. Eng., 24, 587-595 (2007).

Santos, K. G., Murata, V. V., Barrozo, M. A. S. Three-dimensional computational fluid dynamics modeling of spouted bed. Can. J. Chem. Eng., 87, 211-219 (2009).

Vieira, L. G. M., Barbosa, E. A., Damasceno, J. J. R., Barrozo, M. A. S., Performance analysis and design of filtering hydrocyclones. Braz. J. Chem. Eng., 22, 143-152 (2005).

Vieira Neto, J. L., Duarte, C. R., Murata, V. V., Barrozo, M. A. S., Effect of a draft tube on the fluid dynamics of a spouted bed: Experimental and CFD studies. Drying Technol., 26, 299-307 (2008).

Vieira Neto, J. L., Martins, A. L., Silveira Neto, A., Ataíde, C. H., Barrozo, M. A. S., CFD applied to turbulent flows in concentric and eccentric annuli with inner shaft rotation. Can. J. Chem. Eng., 89, 636-646 (2011).